Journal of Power Sources 241 (2013) 46–55

Contents lists available at SciVerse ScienceDirect

Journal of Power Sources

journal homepage: www.elsevier.com/locate/jpowsour

Theoretical and experimental analysis of heat generations of a pouch type $LiMn_2O_4$/carbon high power Li-polymer battery

Meng Xiao*, Song-Yul Choe

Mechanical Engineering, 1418 Wiggins Hall, Auburn Univ., Auburn, AL 36849, USA

HIGHLIGHTS

- Analyzed the two most popular heat generation equations and found out their missing terms.
- Designed a calorimeter to measure the heat generation of a pouch type power cell dynamically.
- A electrochemical-thermal model is validated by the measurement result.

ARTICLE INFO

Article history:
Received 16 February 2013
Received in revised form
8 April 2013
Accepted 11 April 2013
Available online 20 April 2013

Keywords:
Heat generation
Pouch type Li-polymer battery
Electrochemical and thermal model
Enthalpy heating
Heat of mixing

ABSTRACT

Charge transport and chemical reactions during charging and discharging of a battery produce heat that determines temperature behaviors. The elevated temperature causes undesired side reactions that accelerate degradation and potentially result in catastrophic operating conditions like a thermal runaway. The heat generated in an operating battery is generally approximated by the sum of the reversible and irreversible heat. The reversible heat is produced by the change of entropy. The irreversible heat is approximated by either the overpotential heating or Ohmic and reaction heating. Most studies have compared the surface temperature with tuned convection coefficients, but not investigated the heat generation directly. A study conveyed shows that two other heat source terms, enthalpy heating and heat of mixing, should be included to accurately and completely describe the heat generation. The first one is caused by diffusion of lithium ions in the solid phase and the second one by change of the gradient of ion concentrations.

An electrochemical thermal model including these additional terms is experimentally validated against calorimetric measurements on a 15.7 Ah $LiMn_2O_4$/carbon pouch type power cell using a specially designed calorimeter.

1. Introduction

Lithium ion batteries are widely used in transportation and grid applications because of their higher energy and power density compared to other rechargeable batteries. These applications require a long lifespan with low degradation. When a battery is charged and discharged, ions are transported from cathode to anode and vice versa, while electrons flow through an external circuit from one electrode to the other. The charge transport, reduction, and oxidation processes continuously generate heat that can affect these processes and the degradation. Operation of a battery in an elevated temperature accelerates electrolyte and binder decompositions that lead to a capacity fade. In addition, the reaction products can reduce the accessible surface area of the electrode particles, which leads to a power fade [1]. A comparison at elevated operating temperatures from 278 K to 318 K shows that the capacity fade and the power fade rate at 318 K were eight and two times, respectively, higher than those at 278 K [2]. Therefore, battery manufacturers put enormous effort into optimizing the design for the high thermal stability of the materials and less degradation [3]. In addition, temperature affects other parameters like diffusion coefficients, conductivities and reversible heat generation [4]. Moreover, the large amount of heat generated in modules or a pack should be properly rejected to prevent a thermal runaway and minimize the temperature effects on cell performances and degradation [5]. Therefore, accurate estimation of the heat generation rate is crucial not only for the design of the battery, but also for allowing safe operations.

Heat of a battery is described by two source terms, the reversible and irreversible heat. The reversible heat is produced by the change of entropy at an operating cell temperature, which is expressed by a

* Corresponding author. Tel.: +1 334 655 1607; fax: +1 334 844 3307.
E-mail addresses: mzx0001@auburn.edu, xiaomeng996@sohu.com (M. Xiao), choe@auburn.edu (S.-Y. Choe).

0378-7753/$ – see front matter © 2013 Elsevier B.V. All rights reserved.
http://dx.doi.org/10.1016/j.jpowsour.2013.04.062

Nomenclature

c	lithium ion concentration (mol cm^{-3})
j^{Li}	current density(A cm^{-3})
E_{chem}	chemical energy storage (J)
F	Faraday's constant (96,487 C mol^{-1})
I	current (A)
Q_{max}	battery capacity (A h)
Q_{irr}	irreversible heat generation (W)
Q_{rev}	reversible heat generation (W)
R	universal gas constant (8.314 J mol^{-1} K^{-1})
SOC	state of charge (%)
T	cell temperature (K)
U_{equ}	standard potential affected by solid concentration (V)
V	volume (cm^3)
V_t	terminal voltage (V)

Greek symbols

ε	volume fraction in a porous medium (%)
ϕ	potential in a phase (V)
κ	ionic conductivity of electrolyte (S cm^{-1})
κ_D	diffusion conductivity (A cm^{-1})
σ	conductivity of solid active material (S cm^{-1})

Subscripts

+	positive electrode
−	negative electrode
e	electrolyte phase
eff	effective
s	solid phase

product between the change of entropy and the working temperature. On the other hand, the change of the entropy can be expressed using the open circuit voltage (OCV), so the reversible heat can be determined by measuring the open circuit voltage (OCV) when the cell temperature varies and a function of state-of-charge (SOC).

The profile of reversible heat is inherent and depends upon not only materials used for design of electrodes but also their manufacturing processes [6]. Conversely, the irreversible heat sources are a function of the overpotentials with discharging or charging current [7–10]. For the first time, Rao calculated that the irreversible heat is continuously generated even though the current applied to the cell goes to zero. He calculated the enthalpy change in the electrode bulk and found heat generation due to changing rate of ion concentration gradient. This portion is called the heat of mixing is not negligible only when the OCV curve changes rapidly [11]. However, the author did not consider the heat generated in the particles of electrodes along the radial direction. This effect was included by Thomas [12]. In addition, the change of entropy in $LiNi_{0.8}Co_{0.2}O_2$/carbon coin cells at different SOC was measured for the temperature range from 294 K to 302 K using a water bath. However, the results did not show effects of the heat of mixing because the current applied was too low to generate any observable heat of mixing. The principle for this measurement was based on the energy balance, where the heat source was obtained from the difference between the heat exchanged with environment and the heat accumulated that is proportional to battery temperature changing rate. Batteries left in environment of the open air [13,14] can be thermally affected by the surrounding air flow or turbulences and might have a changed convection coefficient that deteriorates the accuracy of the measurement of heat exchange with environment.

Forgeza used two thermal couples. One was inserted into a cylindrical $LiFePO_4$/carbon battery and other was placed at a surface to measure both inside and outside temperatures and to calculate a heat transfer [15]. Seemingly, this method is accurate since the convection coefficient affected by air flows is not used for the measurement, but only works for the cylindrical batteries that allows for placement of a sensor inside of a cell.

Other researchers have used commercial isothermal calorimeters to measure the heat generation rate [8,16]. However, to accommodate the battery geometry the calorimeter cavities must be filled with some materials, which results in a relatively large thermal time constant, so that the measurement of a quick heat generation is not possible. In addition, most commercially available calorimeters are designed for testing thermal stability of materials, so the installed power is not large enough to match the high power battery cell.

Therefore, we have designed a special calorimeter using two thermoelectric devices that allows for dynamic characterization of the heat source terms of a high power cell. The designed calorimeter is firstly calibrated for the $LiMn_2O_4$/carbon pouch type power cell and then used to estimate the heat of mixing dynamically. The electrochemical thermal model developed previously is used to calculate the heat generation and compare with the experimental data [17].

2. Electrochemical and thermal model

2.1. Electrochemical model

The electrochemical model used for this research was first proposed by Doyle [18]. The model assumes that a cell has five layers that are sandwiched; anode current collector, anode, separator, cathode and cathode current collector, as shown in Fig. 1. The electrodes are composed of uniformly distributed spherical particles with electrolyte filling in the gaps between particles as well as the pores in the separator. Chemical reactions take place only at interface between electrodes particles and electrolyte. When charged and discharged, lithium ions generated may be present in both electrolyte and electrodes and diffuse in different directions, while free electrons exist only in the electrode particles. When one electrode releases a given number of lithium ions to the electrolyte the number of free electrons is generated inside the electrode particles, so charge is conserved. The released ions in the electrolyte are transported through the separator and finally end to the

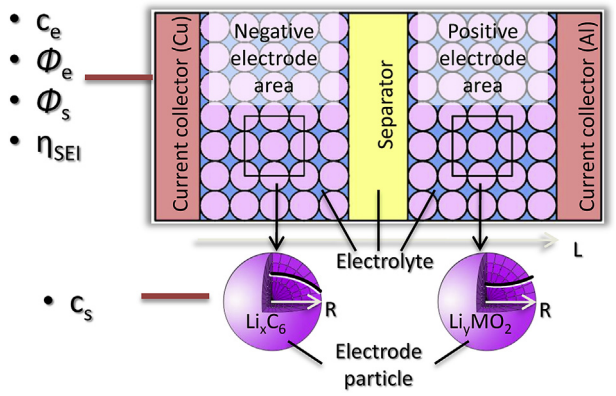

Fig. 1. Setup for modeling of lithium ion battery.

other electrode, while the electrons go through outer circuit to the other electrode, and they combine at the interface between the electrolyte and particles of that electrode.

The equations used for the electrochemical model are summarized below and are discretized in the radial direction (R direction) of particles with 10 and through-the-plane direction (L direction) with 25. The discretized equation is solved with an implicit method and details can be found in a previously published paper [17].

Reaction kinetics

$$j^{\mathrm{Li}} = a_{\mathrm{S}} \cdot i_0 \left(\exp\left(\frac{\alpha_{\mathrm{a}} \cdot n \cdot F}{\mathrm{R} \cdot \mathrm{T}} (\eta - \eta_{\mathrm{SEI}}) \right) - \exp\left(-\frac{\alpha_{\mathrm{c}} \cdot n \cdot F}{\mathrm{R} \cdot \mathrm{T}} (\eta - \eta_{\mathrm{SEI}}) \right) \right) \tag{1}$$

Electrolyte conductive

$$\frac{\partial}{\partial x}\left(\kappa_{\mathrm{e}}^{\mathrm{eff}} \cdot \frac{\partial}{\partial x} \phi_{\mathrm{e}} \right) + \frac{\partial}{\partial x}\left(\kappa_{\mathrm{D,e}}^{\mathrm{eff}} \cdot \frac{\partial}{\partial x} (\ln c_{\mathrm{e}}) \right) + j^{\mathrm{Li}} = 0 \tag{2}$$

Solid conductive

$$\frac{\partial}{\partial x}\left(\sigma^{\mathrm{eff}} \cdot \frac{\partial}{\partial x} \phi_{\mathrm{s}} \right) = j^{\mathrm{Li}} \tag{3}$$

Electrolyte ion transport

$$\frac{\partial (\varepsilon_{\mathrm{e}} c_{\mathrm{e}})}{\partial t} = \frac{\partial}{\partial x}\left(D_{\mathrm{e}}^{\mathrm{eff}} \cdot \frac{\partial}{\partial x} c_{\mathrm{e}} \right) + \frac{1 - t_+^0}{F} j^{\mathrm{Li}} \tag{4}$$

Solid ion transport

$$\frac{\partial c_{\mathrm{s}}}{\partial t} = \frac{D_{\mathrm{s}}}{r^2} \frac{\partial}{\partial r}\left(r^2 \frac{\partial c_{\mathrm{s}}}{\partial r} \right) \tag{5}$$

2.2. Heat generation

2.2.1. Review

The total heat generation in a lithium ion battery (Q_{sum}) is divided into two terms, reversible heat, Q_{rev}, and irreversible heat, Q_{irr}.

$$Q_{\mathrm{sum}} = Q_{\mathrm{rev}} + Q_{\mathrm{irr}} \tag{6}$$

The reversible heat generation is given by Equation (7),

$$Q_{\mathrm{rev}} = -I \cdot T \cdot \frac{\partial U_{\mathrm{OCV}}}{\partial T} \tag{7}$$

where I is the terminal current, which sign is defined as positive when discharged. T is the temperature in the battery and U_{OCV} is the open circuit voltage.

The irreversible heat generation can be expressed by two ways as shown in Equations (8) and (9).

Equation (8) assumes that the voltage difference between the U_{OCV} and terminal voltage includes a sum of all of voltage drops caused by electron and ion transport and chemical reactions, as shown below. Multiplication with the current results in the irreversible heat,

$$Q_{\mathrm{irr}} = I \cdot (U_{\mathrm{OCV}} - V_{\mathrm{t}}) \tag{8}$$

where the open circuit voltage, U_{OCV}, is the function of SOC.

The heat source can be estimated when the U_{OCV} and V_{t} are known. This equation is simple to understand, but the term becomes zero when the current becomes zero, so that the heat of mixing is not considered.

The other formulation for the irreversible heat generation as shown in Equation (9) is also widely used [14,19–24]. The equation includes two terms, the reaction term and Ohmic heating that are derived from the electrochemical formulation,

$$\begin{aligned} Q_{\mathrm{irr}} &= Q_{\mathrm{reaction}} + Q_{\mathrm{ohm}} \\ Q_{\mathrm{reaction}} &= \int j^{\mathrm{Li}} \cdot (\phi_{\mathrm{s}} - \phi_{\mathrm{e}} - U_{\mathrm{equ}}) \cdot \mathrm{d}V \\ Q_{\mathrm{ohm}} &= \int \left[\sigma^{\mathrm{eff}} (\nabla \phi_{\mathrm{s}})^2 + \cdot \left(\kappa^{\mathrm{eff}} \cdot \nabla \phi_{\mathrm{e}} + \kappa_{\mathrm{D}}^{\mathrm{eff}} \nabla \ln c_{\mathrm{e}} \right) \cdot \nabla \phi_{\mathrm{e}} \right] \cdot \mathrm{d}V \end{aligned} \tag{9}$$

where j^{Li} is the current density and defined to be positive for the current from electrode to electrolyte, ϕ_{s} is the electrode potential, ϕ_{e} is the electrolyte potential, σ^{eff} and κ^{eff} are the effective conductivities in electrode and electrolyte and $\kappa_{\mathrm{D}}^{\mathrm{eff}}$ is the effective diffusion conductivity in electrolyte.

Equation (9) does not consider the heat generation by solid phase lithium diffusion that is defined as enthalpy heating [11]. In order to explain the enthalpy heating, chemical energy is introduced, which is defined as the energy stored in a battery by means of chemical reactions.

If the charging and discharging current are low, it can be assumed that the terminal voltage always equals to the OCV and the battery is in quasi-steady state, so no irreversible heat is generated. Then, the chemical energy at a given SOC is defined as the total electrical energy input from 0% SOC to the given SOC,

$$E_{\mathrm{chem}}(\mathrm{SOC}) = \int_0^{\mathrm{SOC}} Q_{\max} \cdot U_{\mathrm{OCV}} \cdot \mathrm{dSOC} \tag{10}$$

where $Q_{\max}$ is the maximum capacity of the battery that is constant. It should be noted that the chemical energy is only a function of SOC.

On the other hand, the enthalpy heating for a particle can be expressed based on the decreasing rate of the chemical energy of the particle and the electric power that the particle produces. The decreasing rate of the chemical energy is a product of the local reaction rate of the particle, j^{Li}, with the average equilibrium potential inside of the particle, U_{avg}, while the electric power is equal to the product of the local reaction rate of the particle, j^{Li}, with the equilibrium potential at the surface of the particle, $U_{\mathrm{s,e}}$. As a result, the enthalpy heating becomes $j^{\mathrm{Li}} \cdot (U_{\mathrm{avg}} - U_{\mathrm{s,e}})$. Transient behavior of enthalpy heating (Blue line) as function of reaction rate (Green line), average equilibrium potential (colorful line) and equilibrium potential at the interface (Black line) in the radial direction is shown in Fig. 2 using the electrochemical model. It is assumed that the battery is discharged with 7 C at $t = 0$, where the initial equilibrium potential is 4.95 V. The reaction rate increases, but not linearly because of the change of ion concentration in L direction, while the equilibrium potential at the interface decreases because of the increased surface concentration until a sudden voltage drop given by OCV. When the discharging current is interrupted, the cell becomes relaxed and gets recovered. Accordingly, the enthalpy heating calculated by multiplication of the reaction rate and potential difference increases relatively slowly at the beginning, drastically and finally returns to zero. The amount of the enthalpy heating can be more than half of total irreversible heat generation.

The heat of mixing is a new source term that is caused by the transient behavior of ion concentrations and the nonlinearity of the equilibrium potentials of electrodes. When the battery is charged and discharged, there is a period of time that the ion concentrations in the particles are not uniformly distributed, so the SOC at every

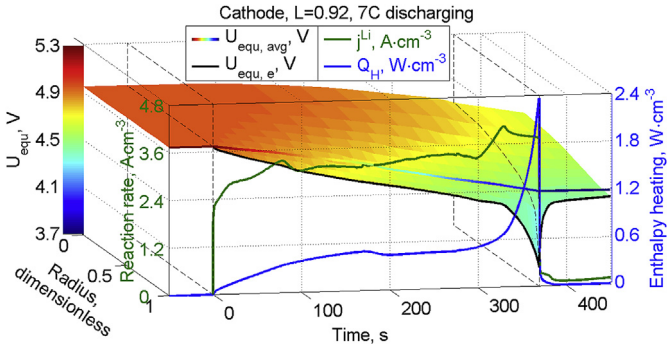

Fig. 2. Transient behavior of enthalpy heating as function of reaction rate and equilibrium potential in the radial direction.

location is different than the given average SOC. As a result, the equilibrium potentials at the every location are different than the equilibrium potential at the average SOC.

$$\left(\overline{U(\mathrm{SOC})} - U\left(\overline{\mathrm{SOC}}\right)\right)\cdot Q_{\max} \tag{11}$$

It is assumed that there are two adjacent control volumes in a particle with concentrations, c_{s1} and c_{s2}, the equilibrium potentials, U_1 and U_2, the average potential, U_{avg}, can be obtained by averaging both U values. After the cell is relaxed, the final potential which is called the mix potential, U_{mix}, might be higher or lower than before because the equilibrium potentials are not linear. The enclosed area between the two different potentials at the given range of concentrations presents the heat of mixing as shown in Fig. 3.

In order to evaluate the Equation (9), the heat generation in a battery for a capacity of 10 Ah is calculated using the parameters given in Ref. [21], where the effect of the reversible heat generation is removed by discharging the battery at 2 C for 360 s, and then charging at 2 C for 360 s.

After the battery has rested long enough, the state is the same as the initial state. The total reversible heat generation is zero, while the total irreversible heat generation is equal to the enclosed area by the terminal voltage for charging and discharging, as shown in Fig. 4(a). The OCV curve separates the hysteresis area into two areas that are exactly the same as that of the irreversible heat generations at the discharging and charging calculated from

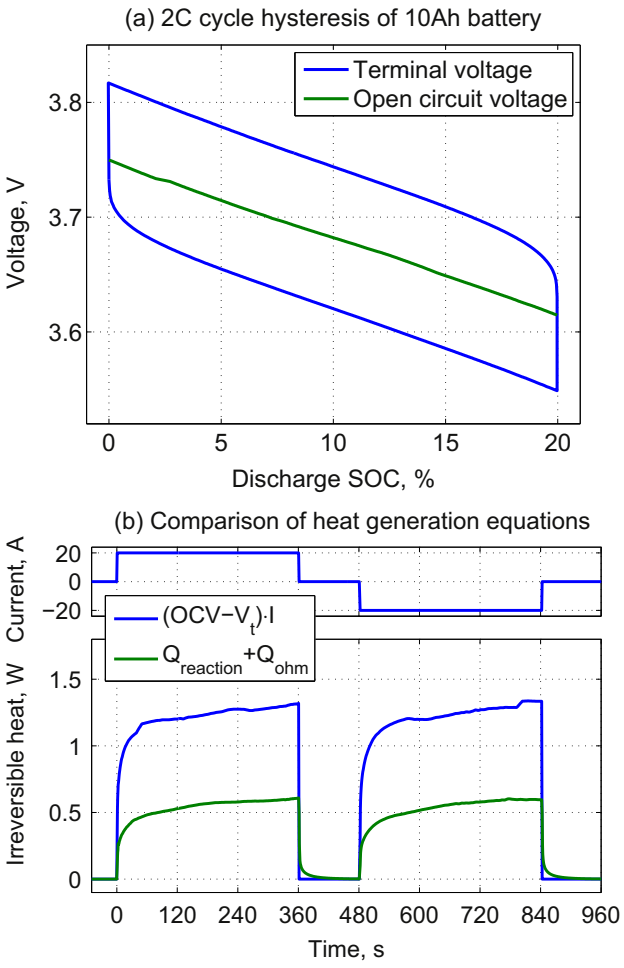

Fig. 4. Simulation of a battery at 2 C charging and discharging.

Equation (8). The amount of the heat generated is 875 J. Conversely, the irreversible heat generation calculated from Equation (9) is a much smaller amount of 390 J that is much less than the previous one, as shown in Fig. 4(b), which is presumably because the calculation using Equation (9) does not include the enthalpy heating. It should be noted that the difference is not negligible.

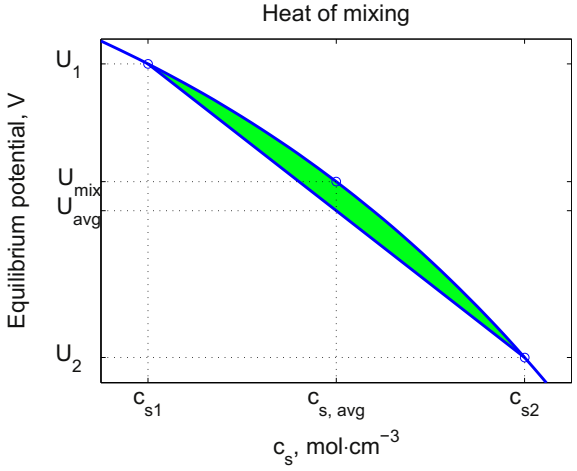

Fig. 3. Heat of mixing.

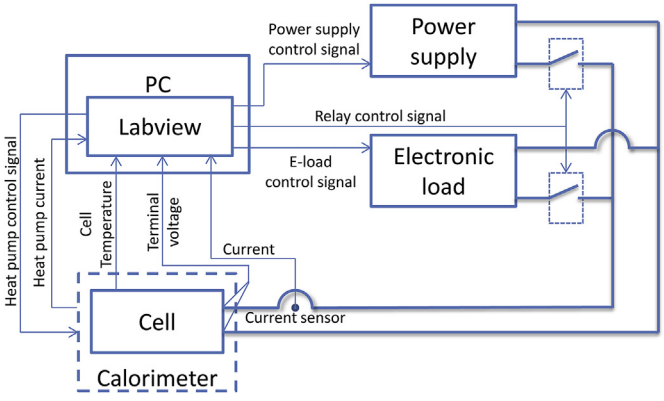

Fig. 5. Experimental setup.

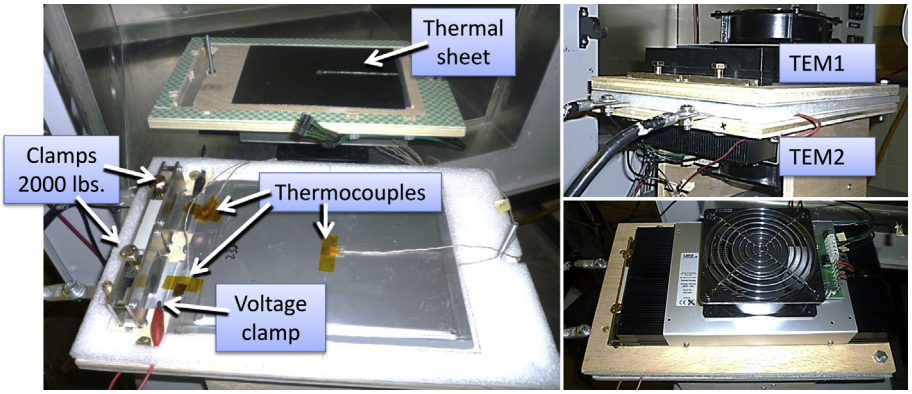

Fig. 6. Calorimeter setup.

2.3. New formulation for irreversible heat generation

The proposed irreversible heat generation considers both the enthalpy heating and the heat of mixing, which is derived from the chemical energy of the battery.

Charging and discharging a battery can be described using energy balances. When a battery is charged, electric energy is transferred from the source to the battery and increases the chemical energy. However, part of the electric energy is dissipated as an irreversible heat. Conversely, when a battery is discharged, the chemical energy of the battery is transferred to the electric energy, while the part of chemical energy is dissipated as a heat, too. When the discharging current is defined to be positive, the irreversible heat generation rate can be expressed using the electric power input and the chemical energy increase rate, as shown in Equation (12),

$$Q_{irr} = -I\cdot V_t - \frac{dE_{chem}}{dt} \tag{12}$$

The chemical energy can be expressed as follows,

$$\frac{dE_{chem}}{dt} = Q_{max}\cdot U_{OCV}(SOC)\cdot\frac{dSOC}{dt} \tag{13}$$

where SOC denotes the average SOC that can be calculated from the ion concentration in the solid phase of both electrodes,

$$\begin{aligned} SOC_- &= SOC = \frac{\overline{c_{s-}} - c_{s-,0\%}}{c_{s-,100\%} - c_{s-,0\%}} \\ SOC_+ &= 1 - SOC = 1 - \frac{\overline{c_{s+}} - c_{s+,0\%}}{c_{s+,100\%} - c_{s+,0\%}} \\ \frac{dSOC_-}{dt} &= \frac{1}{c_{s-,100\%} - c_{s-,0\%}}\frac{dc_{s-}}{dt} \\ \frac{dSOC_+}{dt} &= -\frac{1}{c_{s+,100\%} - c_{s+,0\%}}\frac{dc_{s+}}{dt} \end{aligned} \tag{14}$$

where the c_s is the solid phase ion concentration distribution in the L and R direction in electrodes shown in Fig. 1, $c_{s,100\%}$ and $c_{s,0\%}$ are the solid phase lithium concentration when SOC is 100% and 0%, respectively, and V is the volumes of two electrodes.

Similarly, the maximum capacity, Q_{max}, can be expressed using the solid phase ion concentration,

$$\begin{aligned} Q_{max} &= Q_{max-} = Q_{max+} \\ Q_{max-} &= \varepsilon_{s-}\cdot F\cdot V_-\left(c_{s-,100} - c_{s-,0}\right) \\ Q_{max+} &= \varepsilon_{s+}\cdot F\cdot V_+\left(c_{s+,0} - c_{s+,100}\right) \end{aligned} \tag{15}$$

where ε_s is the active material volume fraction and F is the Faraday constant.

It should be noted that when SOC increases, the lithium ion concentration in the anode increases, while the ion concentration in the cathode decreases, so that they have an opposite sign. On the other hand, the OCV is the difference between the two electrodes equilibrium potentials as follows:

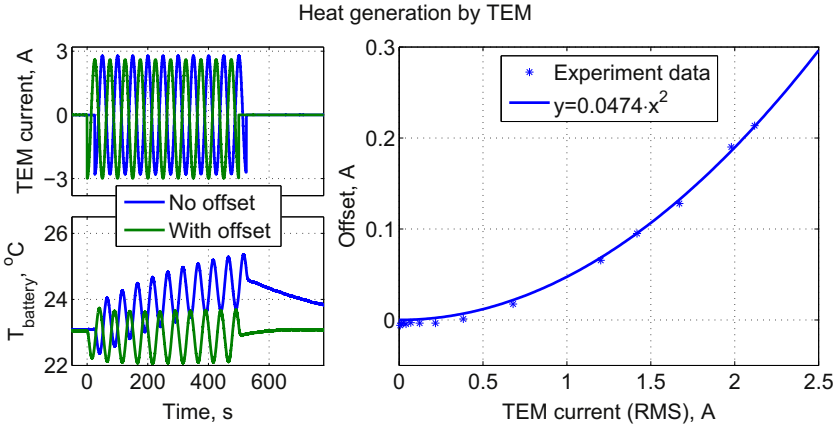

Fig. 7. Heat generation by the TEM.

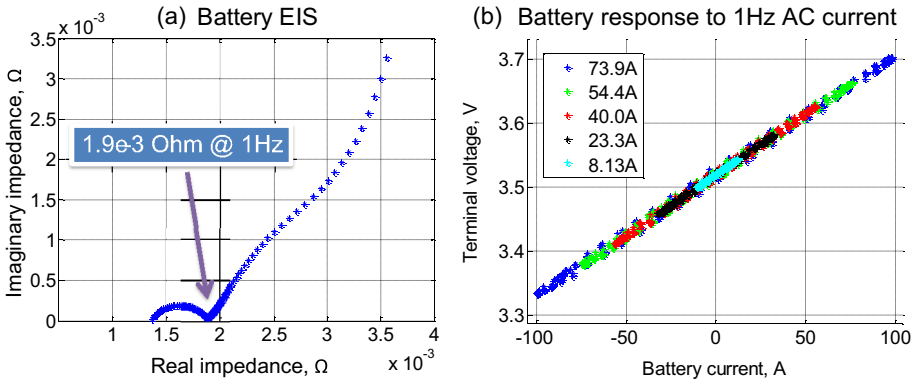

Fig. 8. a) EIS characteristic of the battery b) terminal voltage versus current.

$$U_{OCV}(SOC) = U_{equ+}(c_{s,+}) - U_{equ-}(c_{s,-}) \tag{16}$$

Substituting Equation (12) by (13), (14), (15), (16) and taking into account the non-uniform distribution of solid phase lithium concentration, a new formulation is found for calculation of the irreversible heat generation as follows:

$$Q_{irr} = -I\cdot V_t + F\cdot\varepsilon_{s_+}\cdot\int_{V+} U_{equ+}\cdot\frac{dc_{s+}}{dt}\cdot dV + F\cdot\varepsilon_{s-}\cdot\int_{V-} U_{equ-}\cdot\frac{dc_{s-}}{dt}\cdot dV \tag{17}$$

Hence, the variables of both U_{equ} and c_s are a function of the R and L coordinate. Since the equation is derived from the energy balance and considering the chemical energy that is only a function of SOC, the energy is conserved. In addition, the concentrations that might be present after the terminal current becomes zero represent dynamic behavior of the heat source.

3. Characterization of heat sources

3.1. Design of a calorimeter and test station

Calorimeters are widely used to measure heat generation rates of batteries, but do not provide the dynamics needed for step charging and discharging of cells because of limited heat transfer capability given by cavities and the power needed for cells. A new calorimeter was designed using two thermoelectric devices (TEM) and used to validate the proposing heat generation rate.

When comparing the proposed irreversible heat generation Equation (17) with the conventional Equation (8), the most obvious difference between these two equations is the transient behavior when the load current becomes zero. The first term of Equation (17) disappears, but the other two terms, which represent the heat of mixing, are still present. The heat generated after the interruption is dependent upon the instantaneous concentrations in both electrodes that are functions of the amplitude of the current before the interruption. Therefore, the calorimeter should respond very rapidly and reject a large amount of heat, so that high power heat pumps are required.

The battery used for the experiments is a pouch type power cell with dimension of active materials about 20 cm × 15 cm × 5 mm and made of $LiMn_2O_4$ and carbon. Its capacity is 15.7 Ah and the operating voltage is from 2.5 V to 4.15 V. The test station was constructed using a DC power supply and an electronic load. LabVIEW embedded in a PC was used to control the power supply, the e-load and the TEMs, as depicted in Fig. 5. A high resolution current transformer and four thermocouples were employed to accurately measure the current and the surface temperatures. Two thermocouples were located near the terminal tabs and others were on the both sides of the battery center.

The calorimeter was designed using two TEMs as heat pumps, where the battery is placed between the two TEMs, for which the maximum cooling power is 160 W. Carbon based thermal sheets were used to improve heat conduction between the battery and the

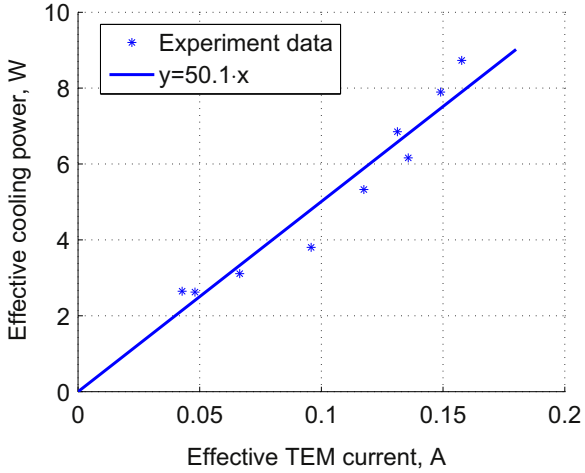

Fig. 9. TEM heat pump constant.

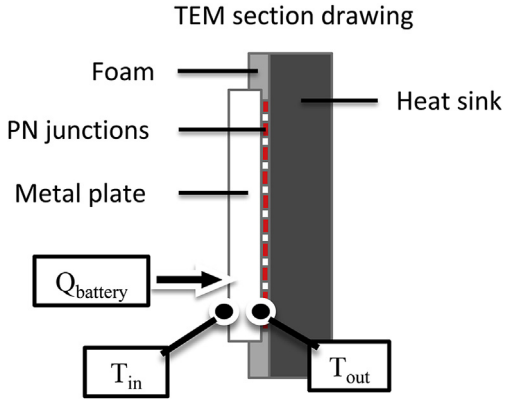

Fig. 10. Structure of TEM.

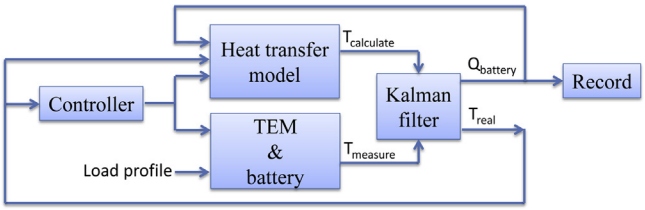

Fig. 11. Kalman filter used to improve dynamic response.

TEMs as shown in Fig. 6. The TEMs are connected in series and powered by a 20 A high frequency bipolar power supply that is controlled by the PC via LabVIEW.

The contacts between the terminal tabs and clamps may have a high resistance and the associated high voltage drop can cause relatively high heat generation, so special attention should be paid to design of the clamps. Experimental tests of the effects of clamping force on contact resistance showed that the forces more than 2000 lbs on each tab produce a minimum contact resistance. In addition, the mechanical stress and heat capacity of the clamp are optimized using ANSYS. The terminal voltage is measured between tabs, so that effects of the contact resistance are excluded.

3.2. Calibration

3.2.1. Static calibration

Before using the calorimeter for characterization of heat sources, calibrations have been conducted with respect to static and dynamic responses.

According to the manufacturer's manual, the heat pump rate of TEM is given as follows,

$$Q_{\text{pump}} = k_1 \cdot I_{\text{TEM}} - k_2 \cdot I_{\text{TEM}}^2 + k_3 \cdot (T_{\text{cool}} - T_{\text{hot}}) \quad (18)$$

where Q_{pump} is the heat pump rate, I_{TEM} is the input current for the TEM, and T_{cool} and T_{hot} are the temperatures on the both sides of TEM. k_1, k_2 and k_3 are the constants that should be determined.

The first, second and third terms represent the heat pump rate, the heat generation, and the heat conduction, respectively. Under the assumption that the operating temperature of the calorimeter is the same as the ambient temperature, the third term becomes zero.

In order to characterize the TEM with respect to the heat generation, an AC input current without an offset is first applied and then the average temperature at the location between the TEMs and battery increases. Since a constant average temperature is desirable for any AC input currents, different DC offset (Green) are added to the input current. The average temperature at the location between the TEMs and battery follows the input currents with a transition behavior caused by cooling and heating behavior of the TEM that compensates the offset, as shown in Fig. 7, while no current is applied to the battery. Based on the experiment data, an empirical equation, Offset = 0.0474 (TEM current)^2, is derived.

The heat pump rate constant can be determined when heat sources and the TEM input current are known. When the battery acts like a pure resistance, the heat generated in the battery can be simply calculated and used to determine the constant.

Impedance of the battery using the electrochemical impedance spectroscopy (EIS) and terminal voltage versus currents are shown in Fig. 8. When the frequency of the current applied is 1 Hz, the imaginary part of the impedance of the battery becomes zero, the battery acts purely resistively with a resistance of 1.9 mΩ. When the amplitude of the current varies for charging and discharging, the terminal voltage follows the amplitude proportionally and the slope is the same as the resistance measured by the EIS.

In addition, heat generation of the clamps, which is regarded as an extra heat transfer from the clamps to the battery, is considered. The amount of the heat transfer is given from the product of temperature difference and the heat transfer coefficient derived from the experimental data, where the temperature difference is the average value of both clamps minus the temperature at the center of the battery. After compensating for the heat generation by the TEM and the effects of the clamps by means of the heat transfer through terminal tabs at a constant heat generation of the battery, a relationship between the input current for the TEM and the heat pump rate that rejects the heat generation is plotted in Fig. 9. The results show that the cooling power produced by the heat pump is proportional to the input currents for the TEM, so that the TEM can be used as an actuator that produces rejecting heat. The heat pump constant is 50.1 W A^{-1}.

3.2.2. Dynamic calibration

When a battery is charged and discharged with currents steps, heat generation rates follow the abrupt changes of the current. In order to estimate the heat generation accurately, the calorimeter is calibrated for a better dynamic response. One phenomenon in the TEM is the delay between the input currents for the TEM and the associated heat pump rate. The TEM is made of P- and N-type semiconductors alternately connected in series and arranged such that the direction of the heat carried is the same as that of carriers moving. The semiconductors are 4 mm thick and cause a delay in a range of several milliseconds when a current is applied to the TEM [25]. However, this delay is not significant. On the other hand, a

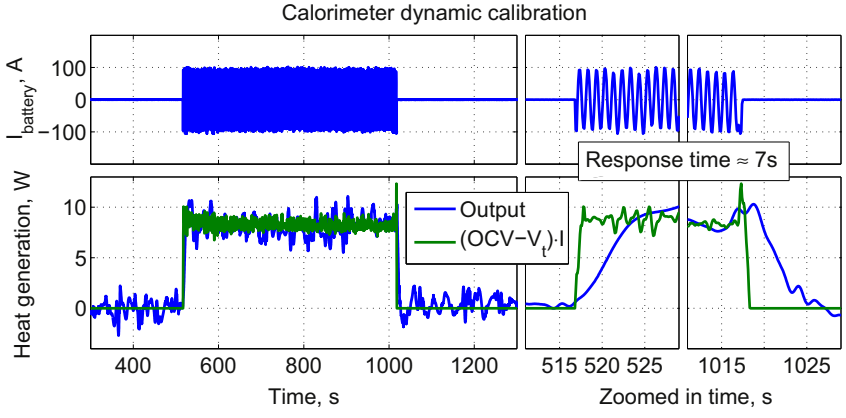

Fig. 12. Dynamic calibration of calorimeter.

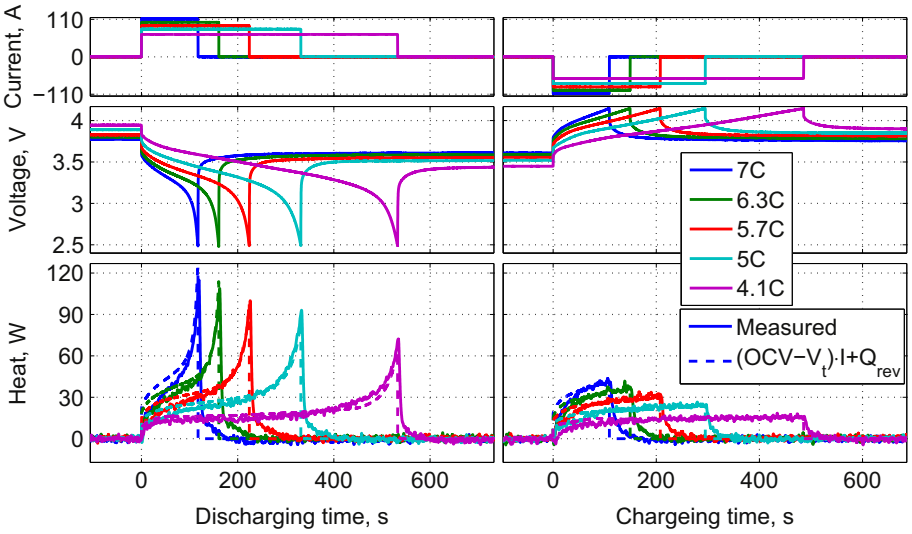

Fig. 13. Heat generation measurements during cycles.

metal plate and a heat sink are mounted to the PN semiconductors of the TEM as shown in Fig. 10, where the metal plate is in contact with the battery.

The limited thermal conductivity and capacitance of the plate cause a time delay that is dominant in the response. In order to improve the dynamic response of the calorimeter, the temperature delay is measured and compensated for using a Kalman filter that requires a dynamic heat transfer model for the plate. The heat transfer model used for estimations is as follows,

$$\frac{\mathrm{d}}{\mathrm{d}t}\begin{pmatrix} T_{\mathrm{in}} \\ T_{\mathrm{out}} \\ Q_{\mathrm{battery}} \end{pmatrix} = A\cdot\begin{pmatrix} T_{\mathrm{in}} \\ T_{\mathrm{out}} \\ Q_{\mathrm{battery}} \end{pmatrix} + B\begin{pmatrix} T_{\mathrm{terminal}} \\ I_{\mathrm{TEM}} \end{pmatrix} \tag{19}$$

where the temperature of the plate on battery side and the semiconductor is T_{in} and T_{out}, respectively, and Q_{battery} is the total heat generated in the battery. T_{terminal} and I_{TEM} denote the temperature at the terminal and the current for TEM, respectively.

Since the T_{in} is the only state variable that can be measured, the other two state variables are estimated using the Kalman filter. Particularly, the Kalman filter is employed to suppress white noise present in the temperature measurements. The diagonal values of the covariance matrix for the filter selected are 10^{-6}, 10^{-6} and 1. The value of the measurement covariance selected is 10^{-4}. A proportional controller is used to avoid overshoot. The schematic diagram for estimation of the variables and controls is shown in Fig. 11.

The calibration results are shown in Fig. 12, where the AC current is applied to the battery and heat generations are plotted. The frequency of the current was 1 Hz and the peak-to-peak amplitude was 200 A. Two heat generation plots are presented, the one from OCV and terminal voltage (green line) and other from the calorimeter (blue line). The former one is calculated for each point as the average overpotential heating in the past cycle (1 s). The plots on the right side show expanded views of the transient behaviors. It takes approximately 7 s for the blue to catch up.

4. Model validation and analysis

The total heat generation is measured when the battery is charged and discharged at different currents in the constant

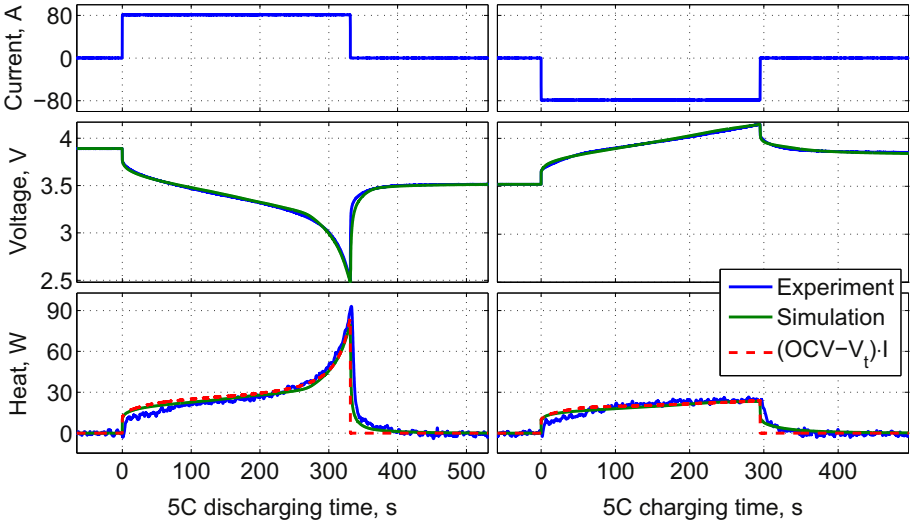

Fig. 14. Comparison between measurement result and model calculation.

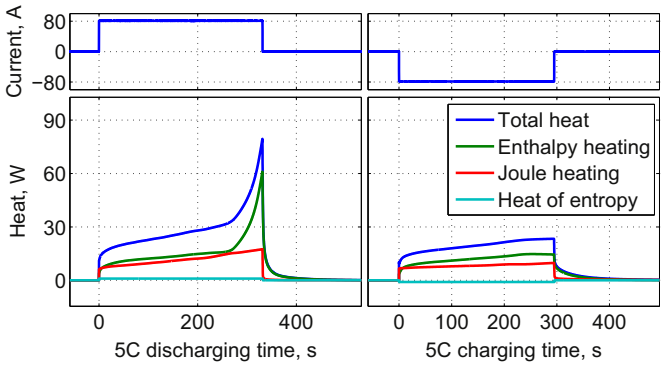

Fig. 15. Simulation of heat source terms.

current (CC) mode. The ambient temperature is set to be 295 K and the maximum temperature rise at the end of 110 A discharge is set to 2.1 K according to the heat capacity and heat conductivity obtained from the dynamic calibration.

Simulated and measured results at different current rates from 4.1 C to 7 C are shown in Fig. 13, where the broken and solid lines represent the calculated data from traditional heat generation Equation (8) under the assumption that the reversible heat generation is constant and the measured data, respectively.

The heat generation rate of the battery at the beginning of charging or discharging is less than those predicted by the calculation. And heat is continuously generated even though the current is equal to zero. The time span of the heat, presumably the heat of mixing, depends on the C rates. A high current results in a long time span. The heat of mixing decays to zero in 1 min when 7 C rate of discharging current is applied even though it only takes 20 s at the 4.1 C charging.

In addition, the total amount of heat generation during charging or discharging is almost the same as that from the beginning to half of the charging and discharging time at the same C rate. By contrast, the heat generation at the end of discharging rises more rapidly than that at the end of charging because the open circuit voltage drops drastically at low SOCs. As a result, the solid phase concentration gradient at the end of discharging is much higher than that at the end of charging. The large concentration gradient leads to a large amount of enthalpy heating.

The current, voltage, and heat generation at the 5 C rate charging and discharging are plotted in Fig. 14, where the simulation results based on the electrochemical model including the proposed heat generation Equation (17) is also added. It should be noted that the heat of mixing that explains the difference between total heat generation and overpotential heating is comparatively small during the constant current charging and discharging, but is not negligible after the current is interrupted.

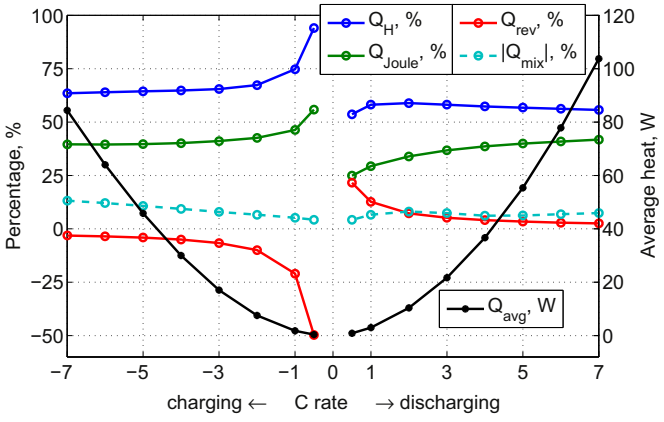

Fig. 16. Analysis of heat source terms at different current rates.

The separated heat source terms are plotted in Fig. 15, which includes the enthalpy heating, Joule heating and heat of entropy. The heat of entropy is the reversible heat that is negligible at this current. The Joule heating shows a similar generation rate as the time elapses. At the beginning of charging and discharging, local conductivities might be different, so that the current flows at spots that have high conductivities. As time elapses, conductivities decrease because of the increased activation overpotential and the current flow is evenly distributed. As a result the Joule heating increases. However, the exchange current density at the low SOC range is smaller than that at high SOC, so the Joule heating at the end of discharging is higher than that at the end of charging. Finally, the enthalpy heating is responsible for the peak at the end of discharge.

The model validated above is used to calculate the individual heat source terms, where the battery is discharged from 4.1 V to 2.5 V and charged from 3.0 V to 4.15 V at different constant C rates. Average actual heat generation and the percentage of the heat over the total heat generation versus the currents is plotted with the black line, as shown in Fig. 16, where the individual terms are also included. Since the average values of heat of mixing are zero, the integration of the absolute value is used for the calculation.

Since reaction and Ohmic heating have a shorter time constant than that of the designed calorimeter, both of them can be measured only as a sum (Joule heating), while the enthalpy heating can be measured alone.

5. Conclusion

Accurate estimation of heat source terms is one of the crucial factors in not only optimizing a battery cell, but also modules and packs. In this paper, a new formulation for the heat generation is proposed that includes the enthalpy heating and heat of mixing. The formulation is incorporated into an electrochemical thermal model and used to analyze heat generation rates.

In order to measure the heat generation dynamically, a new calorimeter was designed using two thermoelectric devices. The calorimeter was statically and dynamically calibrated using EIS and a dynamic error compensator designed based on Kalman filter. Finally, the calorimeter was used to measure the heat generation of a 15.7 Ah $LiMn_2O_4$/carbon pouch type power cell.

Analysis using the model and experimental data shows several findings as follows:

- The reversible heat releases at discharging and absorbs at charging. The amount of the heat is significant at low current, but relatively small at high current;
- Theoretical and experimental analysis shows that the irreversible heat sources in general do not consider either enthalpy heating or heat of mixing. According to simulations, the major contributions to the irreversible heat source are enthalpy heating (55%–70%) and Joule (30%–45%).
- The heat of mixing is zero in average if both of two arbitrary states are steady, but the absolute value of the heat of mixing in average goes up to 13% of the irreversible heat generation. The heat of mixing continuously generates heat and decays to zero in about 1 min after the current is interrupted.

There has been a discrepancy between the simulation and the experimental data within the first 100 s, which might result from the assumption that the transference number is constant. Future

Appendix. Parameters

	Parameter	Negative electrode	Separator	Positive electrode	Unit	Ref.
Design specifications (geometry and volume fractions)	Thickness, δ	50×10^{-4}	25.4×10^{-4}	36.4×10^{-4}	cm	[21]
	Particle radius, R_s	1×10^{-4}		1×10^{-4}	cm	[21]
	Active material volume fraction, ε_s	0.58		0.5		[26]
	Polymer phase volume fraction, ε_p	0.048	0.5	0.11		[26]
	Conductive filler volume fraction, ε_f	0.04		0.06		[26]
	Porosity, ε_e	0.332	0.5	0.33		[26]
Solid and electrolyte phase Li^+ concentration	Maximum solid phase concentration, $c_{s,max}$	40.6×10^{-3}		70.5×10^{-3}	mol cm^{-3}	[a]
	Stoichiometry at 0% SOC: $x_{0\%}$, $y_{0\%}$	0.126		0.936		[b]
	Stoichiometry at 100% SOC: $x_{100\%}$, $y_{100\%}$	0.676		0.442		[b]
	Average electrolyte concentration, c_e	1.2×10^{-3}	1.2×10^{-3}	1.2×10^{-3}	mol cm^{-3}	[26]
Kinetic and transport properties	Exchange current density coefficient, k_{i0}	12.9		6.28	A $cm^{2.5}$ $mol^{-1.5}$	[26]
	Charge-transfer coefficient, α_a, α_c	0.5, 0.5		0.5, 0.5		[18]
	Solid phase Li diffusion coefficient, D_s	1.0×10^{-11}		5.40×10^{-12}	cm^2 s^{-1}	[c]
	Solid phase conductivity, σ	1		0.1	S cm^{-1}	[26]
	Electrolyte phase Li^+ diffusion coefficient, D_e	2.6×10^{-6}	2.6×10^{-6}	2.6×10^{-6}	cm^2 s^{-1}	[26]
	Bruggeman's porosity exponent, p	1.5	1.5	1.5		[27]
	Electrolyte phase ionic conductivity, κ	$2.37c_e \exp(-8983c_e^{1.4})$		$2.37c_e \exp(-8983c_e^{1.4})$	S cm^{-1}	[d]
	Li^+ transference number, t_+^0	0.363	0.363	0.363		[28]

[a] Calculated from capacity, stoichiometry numbers, and battery geometry.
[b] Fitted from initial potential drops at different SOC during charging and discharging.
[c] Fitted from discharge durations measured at different C rates.
[d] Equation is from the Ref. [26] and its coefficients are fitted from overpotentials at different C rates during discharging.

work will include effects of transference number on the heat generation. In addition, design of the calorimeter can be optimized for high resolution measurements even at low current ranges.

References

[1] J. Vetter, et al., J. Power Sources 147 (2005) 269–281.
[2] S. Santhanagopalan, Q. Zhang, K. Kumaresan, R. White, J. Electrochem. Soc. 155 (2008) A345–A353.
[3] D. MacNeil, Z. Lu, Z. Chen, J. Dahn, J. Power Sources 108 (2002) 8–14.
[4] G. Botte, V. Subramanian, R. White, Electrochim. Acta 45 (2000) 2595–2609.
[5] A. Awarke, M. Jaeger, O. Oezdemir, S. Pischinger, Int. J. Energy Res. (2012), http://dx.doi.org/10.1002/er.2884.
[6] V. Viswanathan, et al., J. Power Sources 195 (2010) 3720–3729.
[7] D. Bernardi, E. Pawlikowski, J. Newman, J. Electrochem. Soc. 132 (1985) 5–12.
[8] J. Hong, H. Maleki, S. Al Hallaj, L. Redey, J. Selman, J. Electrochem. Soc. 145 (1998) 1489–1501.
[9] W. Gu, C. Wang, J. Electrochem. Soc. 147 (2000) 2910–2922.
[10] S. Chacko, Y. Chung, J. Power Sources 213 (2012) 296–303.
[11] L. Rao, J. Newman, J. Electrochem. Soc. 144 (1997) 2697–2704.
[12] K. Thomas, J. Newman, J. Power Sources 119–121 (2003) 844–849.
[13] T. Hatchard, D. MacNeil, A. Basu, J. Dahn, J. Electrochem. Soc. 148 (2001) A755–A761.
[14] Y. Ye, Y. Shi, N. Caia, J. Lee, X. He, J. Power Sources 199 (2012) 227–238.
[15] C. Forgez, D. Do, G. Friedrich, M. Morcrette, C. Delacourt, J. Power Sources 195 (2010) 2961–2968.
[16] L. Song, J. Evans, J. Electrochem. Soc. 147 (2000) 2086–2095.
[17] M. Xiao, S. Choe, J. Power Sources 218 (2012) 357–367.
[18] M. Doyle, T. Fuller, J. Newman, J. Electrochem. Soc. 140 (1993) 1526–1533.
[19] K. Kumaresan, G. Sikha, R. White, J. Electrochem. Soc. 155 (2008) A164–A171.
[20] L. Cai, R. White, J. Power Sources 196 (2011) 5985–5989.
[21] K. Smith, C. Wang, J. Power Sources 160 (2006) 662–673.
[22] C. Zhu, X. Li, L. Song, L. Xiang, J. Power Sources 223 (2013) 155–164.
[23] P. Northrop, V. Ramadesigan, S. De, V. Subramanian, J. Electrochem. Soc. 158 (2011) A1461–A1477.
[24] X. Zhang, Electrochim. Acta 56 (2011) 1246–1255.
[25] R. Yang, G. Chen, A. Kumar, G. Snyder, J. Fleurial, Energy Convers. Manag. 46 (2005) 1407–1421.
[26] M. Doyle, Y. Fuentes, J. Electrochem. Soc. 150 (2003) A706–A713.
[27] T. Fuller, M. Doyle, J. Newman, J. Electrochem. Soc. 141 (1994) 1–10.
[28] M. Doyle, A. Gozdz, C. Schmutz, J. Tarascon, J. Newman, J. Electrochem. Soc. 143 (1996) 1890–1903.